Experimental evaluation of polychromatic reconstruction for quantitative CBCT

Michał Walczak, Pascal Paysan, Mathieu Plamondon, and Stefan Scheib

Varian, a Siemens Healthineers Company, Taefernstrasse 7, 5405 Daettwil, Switzerland

ABSTRACT

Polychromatic reconstruction is a promising technique for quantitative cone-beam computed tomography in radiation therapy. In this study, we have implemented polychromatic forward projection into our reconstruction framework to directly reconstruct relative electron density volumes without the need for additional HU calibration. The underlying spectral model takes beam hardening into account by design. Thereby this extended reconstruction framework is a natural step in the direction of spectral imaging, albeit without any hardware modifications. Reconstructed relative electron density volumes from phantom scans show sufficiently good agreement with ground truth for photon dose calculation; relative errors for most inserts are below 3%. We also demonstrate beam hardening artifact reduction in virtual monoenergetic images obtained from polychromatic reconstruction as compared to an established iterative reconstruction using water-based correction. Similarly, polychromatic reconstruction shows potential for mitigating metal artifacts in a clinical scan acquired for a patient with bilateral hip implants.

Keywords: Beam hardening, polychromatic reconstruction, quantitative CBCT

1. INTRODUCTION

High quality cone-beam computed tomography (CBCT) images are essential in image guided radiation therapy for tasks such as soft tissue based patient positioning, structure delineation, and dose calculation. However, due to the polyenergetic nature of X-ray sources, image quality in available single energy reconstructions deteriorates as a result of beam hardening and metal artifacts. Another limitation is that, to determine relative electron density (RED), different HU-RED calibrations are necessary for different acquisition protocols, which is a common obstacle in clinical use. Spectral imaging, e.g., dual energy or photon counting technology, addresses these limitations. However, it generally requires specific hardware solutions. By contrast, leveraging prior knowledge about the polychromatic characteristic of the X-ray beam as well as attenuation properties of different materials can be seen as a middle ground software-based solution. This concept is at the core of polychromatic reconstruction algorithms in the literature.[1–6]

To directly reconstruct RED volumes, we expanded our non-clinical iterative CBCT (iCBCT)[7] reconstruction pipeline (iTools Reconstruction, Varian Medical Systems, Palo Alto, CA, USA) by implementing a polychromatic forward projection that maps RED volume to intensities in projection space, as described by Mason *et al.*[4,5] The core component of the polychromatic forward projection is a piecewise linear approximation of the relation between polychromatic attenuation coefficients and RED values fitted for different materials. Together with an energy-resolved air norm, this polychromatic attenuation model accounts for beam hardening by construction. The model also eliminates the need for using different HU-RED calibrations for different scanning protocols and can be further used to convert reconstructed RED volumes to virtual monoenergetic images (VMI).

Unlike Mason *et al.*,[5] we do not use a polyenergetic kernel-based scatter correction, but instead utilize Acuros® CTS, a polychromatic object scatter estimate based on the linear Boltzmann transport equation,[8,9] available in our iCBCT reconstruction pipeline.

In this paper, we demonstrate that our CBCT reconstruction pipeline augmented with the polychromatic model can be used to reliably determine RED directly. Further, we show the benefits of polychromatic reconstruction for reducing beam hardening artifacts and mitigating metal artifacts, as compared to an established iterative reconstruction method.

7th International Conference on Image Formation in X-Ray Computed Tomography,
edited by Joseph Webster Stayman, Proc. of SPIE Vol. 12304, 123040Y
 · 0277-786X · doi: 10.1117/12.2646455

2. METHOD

2.1 Iterative polychromatic reconstruction

At the core of the iterative polychromatic reconstruction implementation is a polychromatic forward projection, adapted from Mason *et al.*:[4]

$$\mathbf{p}_\alpha = \sum_{j=1}^{N_E} \mathbf{r}_0(E_j) \exp(-[\mathbf{A}\hat{\mu}(\boldsymbol{\rho}_e, E_j)]_\alpha) \tag{1}$$

where $\mathbf{p}_\alpha$ is simulated projection under angle α, $\mathbf{r}_0(E_j)$ is spectral air norm, $\mathbf{A}$ is forward-projection operator, and $\hat{\mu}(\boldsymbol{\rho}_e, E_j)$ is a polychromatic attenuation model transforming the relative electron density volume $\boldsymbol{\rho}_e$ into attenuation coefficients μ. The polychromatic forward projection combines thus prior spectral knowledge about the imaging system (spectral air norm) and material characteristics (polychromatic attenuation model).

The spectral air norm $\mathbf{r}_0(E_j)$ resolves the (energy-integrated) air norm after bowtie filtration $\mathbf{r}_{BT}$ according to spectral characteristics of the imaging system:

$$\mathbf{r}_0(E_j) = \frac{\mathbf{r}_{BT} \circ \mathbf{S}(E_j)}{\sum_{j=1}^{N_E} \mathbf{S}(E_j)} \tag{2}$$

where $\circ$ denotes element-wise product, $\mathbf{S}(E_j)$ is the system sensitivity. It combines source and detector properties:

$$\mathbf{S}(E_j) = I_s(E_j) F_s(E_j) \mathrm{e}^{-\mu_{\mathrm{Ti}}(E_j) l_{\mathrm{Ti}} - \mu_{\mathrm{Al}}(E_j) \mathbf{l}_{\mathrm{Al}}} \eta_d(E_j) E_j \tag{3}$$

where $I_s(E_j)$ is the spectrum flux at the source, $F_s(E_j)$ is inherent filtration at the source, μ_{Ti} and l_{Ti} are respectively attenuation coefficient and thickness of the titanium filter, μ_{Al} and $\mathbf{l}_{\mathrm{Al}}$ are respectively attenuation coefficient and thickness profile of the aluminium bowtie filter, and $\eta_d(E_j)$ is the detector efficiency.

The polychromatic attenuation model takes the form of a piecewise linear fit:[4]

$$\hat{\mu}(\boldsymbol{\rho}_e, E_j) = \sum_{i=1}^{N_f} f_i(\boldsymbol{\rho}_e) \circ [\alpha_i(E_j)\boldsymbol{\rho}_e + \beta_i(E_j)] \tag{4}$$

where $f_i(\boldsymbol{\rho}_e)$ is a material class identification function, $\circ$ denotes element-wise product, $\alpha_i(E_j)$ and $\beta_i(E_j)$ are energy-dependent fit coefficients. The material class identification function maps relative electron density values to corresponding fit segments:[4]

$$f_i(\boldsymbol{\rho}_e) = \begin{cases} 1 & \text{if } k_{i-1} \leq \boldsymbol{\rho}_e \leq k_i \\ 0 & \text{otherwise} \end{cases} \tag{5}$$

where k_i marks a break point between the i and $i+1$ fit segments, with $k_0 = 0$ and $k_{N_f} = \infty$. As described in Mason *et al.*,[4] model parameters $\alpha_i(E_j)$, $\beta_i(E_j)$ and k_i are obtained via a fit to human tissue materials from ICRP Publication,[10] albeit in extended energy range from 15 keV to 140 keV.

Similarly to our established iCBCT reconstruction,[7] for RED volume $\boldsymbol{\rho}_e$ optimization, we use a penalized likelihood cost function with total variation (TV) regularization[11] with a modified expression for the data-fidelity gradient:

$$\nabla_\alpha^{\text{DF-PL}} = \mathbf{A}^{\mathrm{T}}(\mathbf{q}_\alpha - \mathbf{p}_\alpha) \tag{6}$$

where $\mathbf{A}^{\mathrm{T}}$ is the back-projection operator acting on the difference between measured projection $\mathbf{q}_\alpha$ and the polychromatic forward projection $\mathbf{p}_\alpha$ defined in (1). To accelerate the polychromatic reconstruction, we utilize separable quadratic surrogate cost function,[12] ordered subsets,[13] and Nesterov momentum method.[14]

2.2 Reconstruction pipeline

The polychromatic reconstruction pipeline is a natural extension of our iCBCT reconstruction pipeline, which is a two-pass approach.[7] In the first pass of the iCBCT pipeline, the initial HU volume is reconstructed with algebraic reconstruction technique (ART) from fASKS[15] scatter-corrected projections. In the second pass, the initial volume is further refined with statistical reconstruction based on penalized maximum likelihood (PL) using projection images scatter-corrected with Acuros® CTS.

The iterative polychromatic reconstruction (IPR) requires pre-processed projection images. The pre-processing step comprises object and hardware scatter corrections. In our two-pass polychromatic reconstruction pipeline, depicted in Fig. 1, scatter correction is done at two stages. The first pass fASKS scatter correction is carried out identically as in the iCBCT pipeline, and provides input for initial ART reconstruction. In the second pass, scatter correction is done by Acuros® CTS, which consumes the initially reconstructed HU volume to solve the linear Boltzmann transport equation. The scatter-corrected projection images are then fed into IPR to reconstruct the final RED volume.

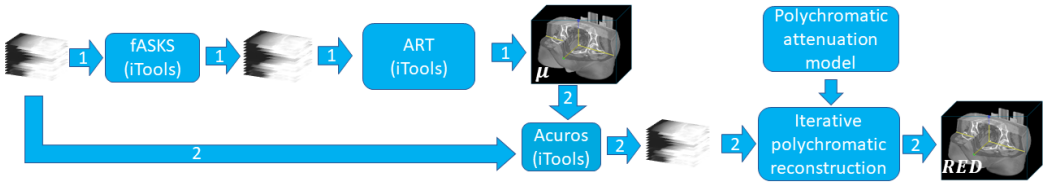

Figure 1: Diagram showing a two-pass polychromatic reconstruction pipeline. In the first pass, algebraic reconstruction technique (ART) consumes projections corrected for scatter with a kernel-based approach (fASKS). HU volume from first-pass provides input for Acuros® CTS scatter correction for subsequent second-pass iterative polychromatic reconstruction (IPR).

3. RESULTS

3.1 Direct RED reconstruction

To demonstrate the use of the polychromatic model for direct RED reconstruction, we scanned the head insert of a CBCT electron density phantom (Model 062MA, Computerized Imaging Reference Systems, Inc., Norfolk, VA, USA) on a Varian Halcyon™ machine (Varian Medical Systems, Palo Alto, CA, USA). The scan was acquired in full-fan geometry at 125 kVp and with kV blades in the longitudinal direction collimated to the height of the phantom electron density plugs. RED volume was reconstructed with 5 initial iCBCT ART iterations, followed by 50 IPR iterations on projections scatter-corrected with Acuros® CTS. Number of iterations was determined empirically for better RED accuracy and image quality.

Central slice through reconstructed RED volume is depicted in Fig. 2a and the resulting difference to ground truth (GT) values relative to water is shown in Fig. 2b. As GT, we assigned nominal RED values from the phantom specification. Mean reconstructed RED values within each plug (areas indicated by dashed circles in Fig. 2a) are listed in Table 1. Except for 'Lung inhale' and 'Dense bone 800' plugs, tissue materials were reconstructed with relative RED error below 3%, thus enabling accurate treatment dose calculation.

3.2 Beam hardening artifact reduction

To illustrate the benefit of polychromatic reconstruction for beam hardening artifact reduction, we scanned the CIRS CBCT electron density phantom with bone inserts (from left to right: solid dense bone 800, solid dense bone 1750, solid trabecular bone 200, solid dense bone 800, solid dense bone 1250) aligned in one row. The phantom was scanned on a Varian Halcyon™ machine in full-fan beam geometry at 125 kVp with kV blades in the longitudinal direction collimated to the insert height for scatter reduction. We compared two reconstructions shown in Fig. 3: a standard iCBCT reconstruction (5 ART iterations, followed by Acuros® CTS scatter correction and 10 PL iterations) and a polychromatic reconstruction (5 iCBCT ART iterations, followed by Acuros® CTS

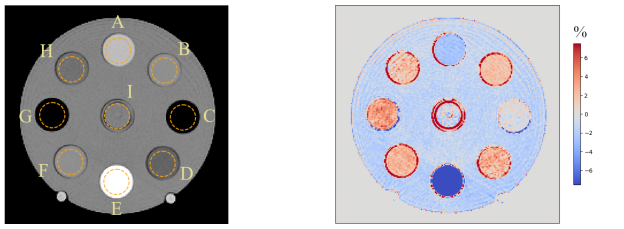

(a) Reconstructed RED (b) Difference to GT relative to water

Figure 2: Central slice of reconstructed RED volume (left; W/L = 0.6/1.0) compared to ground truth (GT) RED (right; W/L = 15/0 %). Positive difference (red) values in right panel denote lower reconstructed values w.r.t. GT. Dashed circles indicate regions for mean RED value calculations.

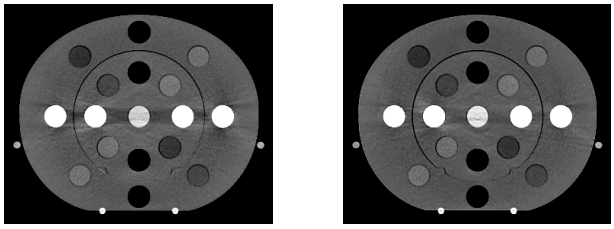

(a) iCBCT (b) VMI (66.5 keV)

Figure 3: Beam hardening artifact near bone plugs is reduced in the VMI from polychromatic reconstruction (right) as compared to an iCBCT reconstruction (left). W/L = 500/75 HU

Table 1: Mean reconstructed RED values for inserts at central slice and their differences to the ground truth (GT) relative to water

Insert	GT RED	reconstructed RED	relative difference %
(A) Trabecular bone 200	1.12	1.146	-2.6
(B) Liver	1.048	1.038	1.0
(C) Lung exhale	0.504	0.505	-0.1
(D) Adipose	0.95	0.937	1.3
(E) Solid dense bone 800	1.441	1.533	-9.2
(F) Muscle	1.051	1.038	1.3
(G) Lung inhale	0.185	0.148	3.7
(H) Breast	0.977	0.967	1.0
(I) Distilled water	1.0	0.999	0.1

scatter correction and subsequent 50 IPR iterations; with number of iterations determined empirically for better RED accuracy and image quality. To compare HU values for both reconstructions, we transformed the RED volume from the polychromatic reconstruction to a VMI using (4) at $E_j = 66.5$ keV, corresponding to the mean beam energy at 125 kVp.

The shading near bone plugs present in the iCBCT reconstruction (Fig. 3a) caused by beam hardening is reduced in the polychromatic reconstruction (Fig. 3b).

3.3 Metal artifact mitigation

We also tested the ability of polychromatic reconstruction to reduce metal artifacts. For that purpose, we selected a scan of a patient with bilateral metal hip implants (data courtesy of Queen's Hospital in Romford). The scan was acquired on a Varian Halcyon™ machine in half-fan beam configuration at 125 kVp. We compared three reconstructions shown in Fig. 4: a standard iCBCT reconstruction (5 ART iterations, followed by Acuros® CTS scatter correction and 5 PL iterations), an iCBCT reconstruction with metal artifact reduction (MAR) and a polychromatic reconstruction (5 iCBCT ART iterations, followed by Acuros® CTS object scatter correction and subsequent 25 IPR iterations). To compare HU values for both reconstructions, we transformed the RED volume from the polychromatic reconstruction to a VMI at $E_j = 74.5$ keV. The polychromatic model used for this reconstruction was extended by a fit to common hip replacement alloys[16] in addition to typical human tissues[10] and comprised of $N_f = 4$ segments.

The shading between hip joints caused by metal implants visible in the iCBCT reconstruction (Fig. 4a) is reduced in the VMI from the polychromatic reconstruction (Fig. 4b), improving the visibility of the bladder. Some level of metal artifacts still remains, however, we point out that, unlike in the iCBCT MAR reconstruction (Fig. 4c) the result of the polychromatic reconstruction is based solely on the underlying polychromatic model without metal inpainting in projections.

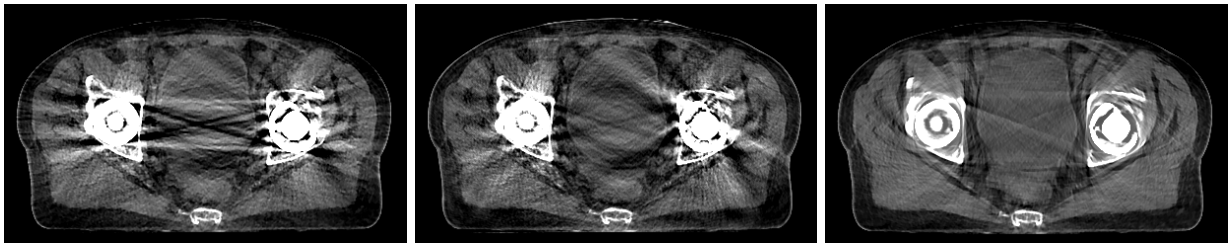

(a) iCBCT (b) VMI (74.5 keV) (c) iCBCT MAR

Figure 4: Metal artifact within bladder region is reduced in the VMI from polychromatic reconstruction (middle) as compared to a standard iCBCT reconstruction (left). As a reference, an iCBCT reconstruction with heuristic metal artifact reduction (MAR) is shown on the right. W/L = 500/75 HU. Patient data courtesy of Queen's Hospital in Romford

4. CONCLUSION

We have implemented physics-based polychromatic forward projection within our CBCT reconstruction pipeline. Preliminary results on phantom data demonstrate the potential of iterative polychromatic reconstruction for direct RED volume reconstruction with reduced beam hardening artifacts. In the presence of metal implants, polychromatic reconstruction helps to improve the visibility of soft tissue by partially removing shading. However, a certain level of metal artifacts persists. We presume metal artifact reduction with polychromatic reconstruction can be further improved by adapting Acuros® CTS object scatter correction implementation to take RED volumes directly as input and extend its material types to include titanium as well. We also see the combination of polychromatic reconstruction with metal inpainting in projections as a potential investigation direction to enable reliable structure auto segmentation and dose calculation for adaptive radiation therapy.

Acknowledgment

The authors would like to thank Queen's Hospital in Romford for providing the patient data.

REFERENCES

[1] De Man, B. et al., "An iterative maximum-likelihood polychromatic algorithm for CT," *IEEE transactions on medical imaging* **20**(10) (2001).

[2] Elbakri, I. A. and Fessler, J. A., "Statistical image reconstruction for polyenergetic x-ray computed tomography," *IEEE transactions on medical imaging* **21**(2) (2002).

[3] Elbakri, I. A. and Fessler, J. A., "Segmentation-free statistical image reconstruction for polyenergetic x-ray computed tomography with experimental validation," *Physics in Medicine and Biology* **48**(15) (2003).

[4] Mason, J. H. et al., "Polyquant CT: direct electron and mass density reconstruction from a single polyenergetic source," *Physics in Medicine & Biology* **62**(22) (2017).

[5] Mason, J. H. et al., "Quantitative cone-beam CT reconstruction with polyenergetic scatter model fusion," *Physics in Medicine & Biology* **63**(22) (2018).

[6] Trotta, L. D. S. et al., "Beam-hardening corrections through a polychromatic projection model integrated to an iterative reconstruction algorithm," *NDT & E International* (2021).

[7] Peterlik, I. et al., "Reducing residual-motion artifacts in iterative 3D CBCT reconstruction in image-guided radiation therapy," *Medical Physics* **48**(10) (2021).

[8] Maslowski, A. et al., "Acuros CTS: A fast, linear Boltzmann transport equation solver for computed tomography scatter–Part I: Core algorithms and validation," *Medical physics* **45**(5) (2018).

[9] Wang, A. et al., "Acuros CTS: A fast, linear Boltzmann transport equation solver for computed tomography scatter–Part II: System modeling, scatter correction, and optimization," *Medical physics* **45**(5) (2018).

[10] ICRP, "Adult reference computational phantoms," *Ann ICRP* **39** (2009).

[11] Rudin, L. I. et al., "Nonlinear total variation based noise removal algorithms," *Physica D: nonlinear phenomena* **60**(1-4) (1992).

[12] Erdogan, H. and Fessler, J. A., "Monotonic algorithms for transmission tomography," in [*5th IEEE EMBS International Summer School on Biomedical Imaging, 2002.*], IEEE (2002).

[13] Kim, D. et al., "Combining ordered subsets and momentum for accelerated X-ray CT image reconstruction," *IEEE transactions on medical imaging* **34**(1) (2014).

[14] Nesterov, Y., "Smooth minimization of non-smooth functions," *Mathematical programming* **103**(1) (2005).

[15] Sun, M. and Star-Lack, J., "Improved scatter correction using adaptive scatter kernel superposition," *Physics in Medicine & Biology* **55**(22) (2010).

[16] Bazalova, M. et al., "Monte Carlo dose calculations for phantoms with hip prostheses," in [*Journal of Physics: Conference Series*], **102**(1), IOP Publishing (2008).